IEEE Access
Multidisciplinary ⋮ Rapid Review ⋮ Open Access Journal

Received 28 June 2022, accepted 19 August 2022, date of publication 25 August 2022, date of current version 2 September 2022.

Digital Object Identifier 10.1109/ACCESS.2022.3201559

RESEARCH ARTICLE

Time Reversal Communications With Channel State Information Estimated From Impedance Modulation at the Receiver

K. BRAHIMA YEO, CECILE LECONTE, PHILIPP DEL HOUGNE, (Member, IEEE), PHILIPPE BESNIER, (Senior Member, IEEE), AND MATTHIEU DAVY

CNRS, IETR-UMR 6164, INSA Rennes, Université de Rennes 1, 35000 Rennes, France

Corresponding author: K. Brahima Yeo (katiembieyaha-brahima.yeo@insa-rennes.fr)

This work was supported in part by the European Union through the European Regional Development Fund (ERDF), in part by the French Region of Brittany and Rennes Métropole through the CPER Project SOPHIE/STIC & Ondes, in part by the Pôle d'Excellence Cyber (PEC), and in part by the French ''Agence Nationale de la Recherche'' under Grant ANR-17-ASTR-0017. The work of Matthieu Davy was supported by the Institut Universitaire de France.

ABSTRACT We determine the channel state information (CSI) of a multiple-input single-output (MISO) Rayleigh channel without prior communications between the transmitting antennas and the receiver. Our approach solely relies on an impedance modulation at the receiver and therefore circumvents the vexing need of a direct feedback between receiver and transmitters. We extract the wavefront to be transmitted in order to achieve optimal focusing on the receiver from a generalized Wigner-Smith operator (WSO). The latter is evaluated based on the scattering matrix of the transmit array measured in the two possible states of the receiver. Based on the CSI extracted via the WSO, any desired precoding technique can be implemented. Here, we show through in-situ time-domain measurements in a reverberation chamber that our approach closely reaches time-reversal performances in terms of focusing efficiency. We expect our approach to open up new perspectives for future wireless communications and wireless power transfer, including applications in the biomedical domain and electronic warfare.

INDEX TERMS Time reversal communications, channel state information, Wigner-Smith operator, multiple-input single-output (MISO), reverberation chamber.

I. INTRODUCTION

Precoding techniques are nowadays routinely exploited in multiple input-multiple output (MIMO) wireless communication systems to assure a high quality-of-service with low energy consumption. When the channel state information (CSI) between transmitting and receiving antennas is estimated and known at the transmitter, the incident wave can be judiciously shaped in space and time in order to fully exploit the spatial diversity and bandwidth of the antenna array and dramatically enhance the data-rate transmission. Several precoding techniques exist, each with their own advantages and limitations. For narrowband signals, the maximum ratio transmission (MRT) is an optimal precoding scheme providing maximally focused intensity on the targeted antenna [1]. In contrast, the zero-forcing technique proposes to annihilate the signal over non-targeted antennas to maximize the signal-to-noise ratio spatially, minimizing multi-user interference [2].

For broadband signals, the multiple-input multiple-output orthogonal frequency division multiplexing (MIMO-OFDM) has been introduced in the past years to achieve an excellent high-rate transmission. This technique is also a great way to counteract multipath fading and other channel impairments. Indeed, the performance of MIMO-OFDM techniques has been highlighted in several wireless standards such as wireless local area networks (WLAN), wireless metropolitan area networks (WMAN) and fourth-generation mobile cellular [3]. Time-reversal (TR) techniques introduced in ultrasonics [4] and transposed to electromagnetic waves [5] were also

The associate editor coordinating the review of this manuscript and approving it for publication was Wei-Wen Hu.

rapidly considered as a new paradigm for energy-efficient communication techniques for wideband or ultra-wide band signals [6], [7], [8], [9]. TR provides an optimal focusing gain in a complex scattering environment [5], [10], [11] with signals that are temporally compressed into a short pulse. This thereby considerably reduces the inter-symbol interference (ISI) at high symbol rates despite lengthy channel impulse responses. The transmission gain can be further enhanced using the one-bit TR technique [12], [13], [14], [15] for which the amplitude of the transmitted signal is normalized positively or negatively according to the sign of the time-reversed signal. The equal gain transmission (EGT) [16] and the TR techniques in the frame of MISO-OFDM communications [17], [18] have been confirmed as the most efficient transmission techniques due to their simple processing compared to MRT. For massive MISO systems, the TR technique outperforms the EGT scheme [19], approaching the performances of the MRT precoding scheme. According to the literature, TR precoding for MISO-OFDM communication systems is an excellent way to ensure efficient and secure communication link thanks to its time and space focusing properties.

A prerequisite of these precoding techniques is the knowledge or at least accurate estimation of the CSI, i.e. the space-time transfer matrix between transmitter and receiver, at the transmitter. The CSI requires a feedback from the receiver to the transmitter which is obtained by transmitting pilots on the reverse link. Many sources of pilot contamination (non-orthogonality of pilot signals, hardware impairments, non-reciprocal transceivers…) may however degrade the estimation of the CSI and therefore the efficiency of precoding schemes [20]. Moreover, the estimation of the CSI is even more challenging for backscatter communications including radio-frequency identification (RFID) technologies. The tag reflects the incoming signal transmitted by the reader and modulates its own impedance to transmit information by changing the phase and amplitude of reflected signals. As the tag does not actively emit waves, no direct feedback is possible which limits, at first sight, the scope of precoding techniques.

In this article, we introduce a technique to estimate the CSI without any direct measurement between the transmitting antenna array and a receiver. Instead, we leverage a modification of the receiving antenna's impedance and demonstrate that the CSI can then be indirectly retrieved. Our approach is based on the Wigner-Smith operator [21], [22] and more precisely on its generalized formulation [23], [24] to extract wavefronts that provide optimal focusing on a target undergoing a modification. The transmission vector between an antenna array and the receiver is reconstructed in amplitude and phase from the eigenvector associated with the most sensitive eigenvalue of the generalized Wigner-Smith (GWS) operator. Our approach is general and is especially efficient within disordered media, here a reverberation chamber with high Q-factor. Because the technique is established in the harmonic domain, we reconstruct the temporal impulse responses giving maximal focusing for wideband signals by correcting a global phase of the optimal eigenvector. We apply a TR precoding scheme to wideband MISO wireless communications and demonstrate an accurate transmission of an image between a transmitting antenna array and a receiving antenna without any direct measurement of the impulse response between them.

The rest of this article is organized as follows. Sec. II is devoted to the theory of the GWS operator and the time-domain definition of its associated optimal wavefront. Sec. III describes our experimental setup involving a reverberation chamber as a propagation environment. We provide evaluate the focusing performance of our proposed technique based on in-situ measurements. Finally, as a proof of concept, we apply our proposed precoding technique to wirelessly transfer a binary image to a non-cooperative receiver that modulates its impedance. We draw conclusions in Sec. IV and outline directions for future work.

II. GENERALIZED WIGNER-SMITH OPERATOR

We consider an array of N transmitting antennas and measure the $N \times N$ scattering matrix $S(\omega)$ built upon transmission and reflection coefficients between each element of the array. These measurements of $S(\omega)$ are carried out for two states of the impedance of the receiver, $S_1(\omega)$ and $S_2(\omega)$ and we seek to extract the vector of transmission coefficients between the transmitting array and the receiver. Our approach relies on the GWS operator recently introduced in the context of wavefront shaping to design wavefronts with optimal properties in the near-field of a target.

In its original form, the Wigner-Smith operator was introduced to study the time delays of particle collisions in quantum mechanics [21], [22] and involves the derivation of the scattering matrix $S(\omega)$ with respect to frequency:

$$Q(\omega) = -iS^{-1}\frac{\partial S}{\partial \omega}. \tag{1}$$

This operator $Q(\omega)$ provides the fullest account of time delays of scattering modes and generalizes the single channel time-delay between transmitting mode n and receiving mode m, $\tau_{mn} = \partial\phi_{mn}/\partial\omega$, where ϕ_{mn} is the phase of the scattering coefficient $S_{mn}(\omega)$, to the complete scattering matrix. The time-delay eigenstates found from a diagonalization of $Q(\omega)$ are insensitive to frequency shifts and are associated with well-defined time delays between incoming and outgoing modes given by the corresponding eigenvalues. In the context of wavefront shaping, these eigenstates make it possible to excite particle-like states in cavities [25], principal modes arriving temporally unscattered in optical fibers [26] or maximally resonant states that maximize energy storage in resonators [27], [28]. This operator may also be useful to shed light on the group delay analysis of microwave devices and the frequency sensitivity of multiport antennas, as illustrated in recent papers [29], [30].

The Wigner-Smith operator has recently been extended to the derivative of S with respect to any global or local

parameter α [23], [24]:

$$Q_\alpha = -iS^{-1}\frac{\partial S}{\partial \alpha}. \tag{2}$$

Similarly to proper time-delays, the eigenvalues of Q_α indicate the global modification of the corresponding eigenstate for a change in α. This approach has been utilized to optimally apply a force to a movable scatterer [23], an angular momentum to a target in rotation, or to maximize the integrated intensity on a target with modified dielectric constant [24]. The incident wavefront for optimal manipulation is provided by the left eigenvector of Q_α associated with the optimal eigenvalue. When α is the modulation of an antenna's impedance, the optimal eigenvector provides maximal focusing on this antenna [31] so that a direct measurement of the transfer function is not anymore required, in contrast to conventional TR techniques. Using the GWS operator, we have also demonstrated maximal focusing on an impedance change within a cable network [32].

A. MONOCHROMATIC GWS

In our case, α is the impedance of the receiver and $\partial S/\partial\alpha$ is estimated from $\Delta S(\omega) = S_1(\omega) - S_2(\omega)$, so that (2) writes $Q_\alpha = -iS_1(\omega)^{-1}\Delta S(\omega)$. We perform a diagonalization of $Q_\alpha(\omega)$ as $q_n^\dagger(\omega)Q_\alpha(\omega) = \theta_n(\omega)q_n^\dagger$, with θ_n and q_n being the eigenvalues and corresponding $N \times 1$ eigenvectors normalized with respect to $\|q_n\| = 1$. The eigenvalues are sorted with respect to their amplitudes. When the typical dimensions of the target are small relative to the wavelength, the first eigenvector (associated with the largest eigenvalue) can be identified as the optimal wavefront for providing maximal intensity to the target: $\psi_{\text{opt}}(\omega) = q_1$. Apart from a global phase shift $\phi(\omega)$, $\psi_{\text{opt}}(\omega)$ is hence theoretically equal to the phase-conjugate of the transmission vector $T(\omega)$ between the transmitting antennas and the receiver:

$$\psi_{\text{ref}}(\omega) = \frac{T^*(\omega)}{\|T(\omega)\|}e^{i\phi(\omega)}. \tag{3}$$

B. TIME-COHERENT POLYCHROMATIC GWS

The optimal wavefront can be determined at each frequency over the bandwidth but the global phase is still unknown. If $\psi(\omega)$ is an eigenvector of $Q(\omega)$, $\psi(\omega)e^{i\phi(\omega)}$ is indeed also an eigenvector associated with the same eigenvalue for any value of $\phi(\omega)$. This a priori precludes a complete estimation of the vector of impulse responses $T(t)$ from the inverse Fourier transform of $\psi_{\text{opt}}(\omega)$ and hence a time-coherent deployment of GWS-based focusing wavefronts.

To overcome this issue and determine the global phase for each frequency, we assume that, in the approximation of a point-like receiver, the transmission vector $T(\omega)$ is proportional to the vector of Green's functions between the transmitting antennas and this target. The matrix $\Delta S(\omega)$ giving the contribution of the target to $S(\omega)$ can then be expressed as

$$\Delta S(\omega) = T(\omega)a(\omega)T^T(\omega). \tag{4}$$

The coefficient $a(\omega)$ is related to the reflectivity associated with the impedance modulation. For non-dispersive targets, when the wave is maximally focused, the receiver behaves as a virtual source that re-emits the incident signal. For an incident wavefront $T^*(\omega)$, its contribution to the received vector $\psi_{\text{out}}(\omega) = \Delta S(\omega)T^*(\omega)$ on the antenna array is proportional to $T(\omega)$: $\psi_{\text{out}}(\omega) \propto T(\omega)$. The phase of $T^\dagger(\omega)\Delta S(\omega)T^*(\omega)$ is therefore equal to 0. This condition provides a framework to correct the global phase $\phi(\omega)$ of $\psi_{\text{opt}}(\omega)$. For each frequency within the bandwidth, $\phi(\omega)$ is determined using

$$\arg[\psi_{\text{opt}}^T(\omega)\Delta S(\omega)\psi_{\text{opt}}(\omega)] = 0. \tag{5}$$

This gives a first condition on $\phi(\omega)$ but an uncertainty remains since both $\phi(\omega)$ and $\phi(\omega)+\pi$ satisfy this equation. We finally assume that the frequency steps over the bandwidth are sufficiently small and rely on the continuity of the phase over the bandwidth to remove π-phase shifts.

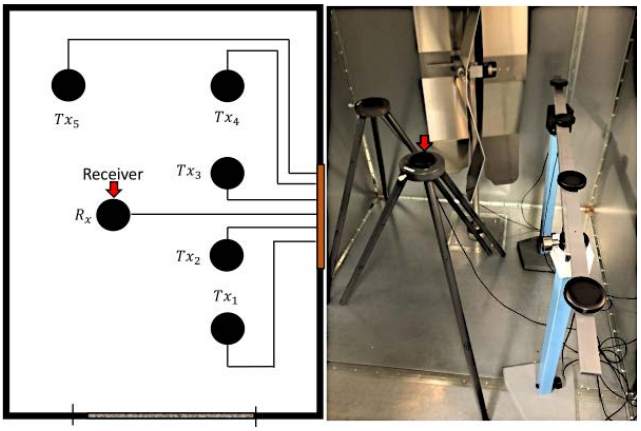

FIGURE 1. Drawing of the measurement setup (left) and picture of the experiment (right). There are 5 transmitted antennas and a receiver inside the reverberation chamber. The receiver is connected or not to port 6 of the VNA (switching the antenna impedance between matched load and open-circuit conditions) in the two measurements of the scattering matrix. Antennas are spaced from each other and from the cavity walls by a minimum of $\lambda/2$, where λ is the largest working wavelength, to avoid unwanted coupling.

III. EXPERIMENTAL RESULTS

A. EXPERIMENTAL SETUP

Measurements are carried out in a $1.5 \times 1.5 \times 2\,m^3$ reverberation chamber in the 700–900 MHz frequency range. The corresponding 200 MHz bandwidth is sampled over 10^4 points giving a sampling frequency $\Delta f = 20\,kHz$. We estimate that the reverberation time of the cavity is $\tau = 150\,ns$, giving a Q-factor of 754. The disordered reverberant environment can be considered to yield channels following Gaussian statistics. In particular, the modulus of any rectangular component of the electric field strength follows a Rayleigh distribution [33]. The antenna array is composed of $N = 5$ antennas with a minimum distance of half-a-wavelength (at 700 MHz) between the elements to minimize unwanted coupling between them. The antennas are connected to 5 ports of a vector network analyzer (VNA) of type Keysight M9005A. It is used to

sense the scattering matrix of the transmit array. The VNA supplies a continuous wave of pulsation ω (over a time window inversely proportional to the IF bandwidth) at a single port and measures the received signal at all ports to retrieve the corresponding line of the scattering matrix. The $N \times N$ scattering matrices $S_1(\omega)$ and $S_2(\omega)$ are measured for two states of the receiver, which consists of the sixth antenna placed inside the cavity, as presented in Fig. 1. The target's diameter is $\lambda/5.4$ so that it can be considered as point-like. The receiver is first disconnected from the VNA, giving an open-circuit condition. In its second state, the receiver is connected to the sixth port of the VNA to mimic a matched-load impedance. This procedure also makes it possible to measure the $N \times 1$ transmission vector $T(\omega)$ between the transmitting antennas and the receiver. This is solely done to compare the results given by the GWS operator for in-situ focusing with a conventional time-reversal operation.

Spectra of the eigenvalues of $Q_\alpha(\omega)$ are presented in Fig. 2(a) on a dB-scale. We observe that the first eigenvalue clearly dominates the other ones with an average amplitude ratio between the first two eigenvalues equal to 34 dB. The scattered field within the reverberation chamber is hence clearly sensitive to the impedance modulation of the receiving antenna. As seen in Fig. 2(b), while the variations of the global phase directly extracted from the diagonalization strongly differs from the one of $T^*(\omega)$, the global phase of $\psi_{\text{opt}}(\omega)$ perfectly matches the expected result once the correction procedure is applied.

To validate our approach and illustrate the correspondence between $\psi_{\text{opt}}(\omega)$ and $T^*(\omega)/\|T(\omega)\|$, we compare the focused intensity found synthetically from VNA measurements using $\psi_{\text{opt}}(\omega)$ to the result of a TR operation. In the spectral domain, the field at the receiver when the incident wavefront $\psi_{\text{opt}}(\omega)$ is transmitted is

$$Y_{\text{opt}}(\omega) = T^T(\omega)\psi_{\text{opt}}(\omega). \tag{6}$$

As a reference, the incoming wavefront for maximum focusing in a time-reversal experiment is obtained from

$$Y_{\text{ref}}(\omega) = |T^T(\omega)\frac{T^*(\omega)}{\|T(\omega)\|}|^2 = \|T(\omega)\|^2. \tag{7}$$

We then perform an inverse Fourier transform of $Y_{\text{opt}}(\omega)$ and $Y_{\text{ref}}(\omega)$ yielding $Y_{\text{opt}}(t)$ and $Y_{ref}(t)$. The results are shown in Fig. 3 and confirm that $Y_{\text{opt}}(t)$ closely corresponds to the time reversal result $Y_{\text{ref}}(t)$. The correlation coefficient between them is equal to 0.998. The TR technique fully exploits the reverberation within the cavity to generate high amplitude pulses focused both in space and time. We have therefore demonstrated the capacity to extract the signal giving perfect focusing without directly measuring the transfer function (CSI) but only by leveraging the modulation of the receiver's impedance.

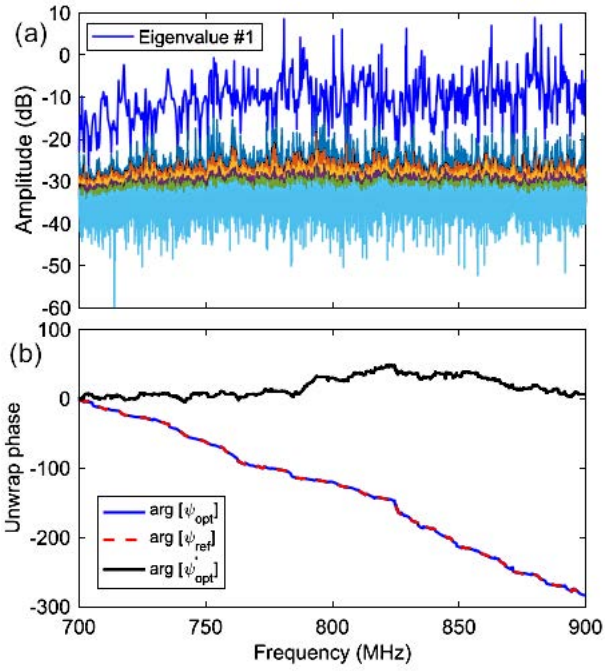

FIGURE 2. (a) Variations of the magnitude of the eigenvalues of Q_α between 700 MHz and 900 MHz. The eigenvalue shown as blue solid line is the highest according to the ranking of eigenvalues in decreasing order. (b) The corrected global phase of the first eigenvector (blue line) perfectly matches that of $T^*(\omega)$ (red dashed line). The uncorrected phase (black solid line) is shown for comparison.

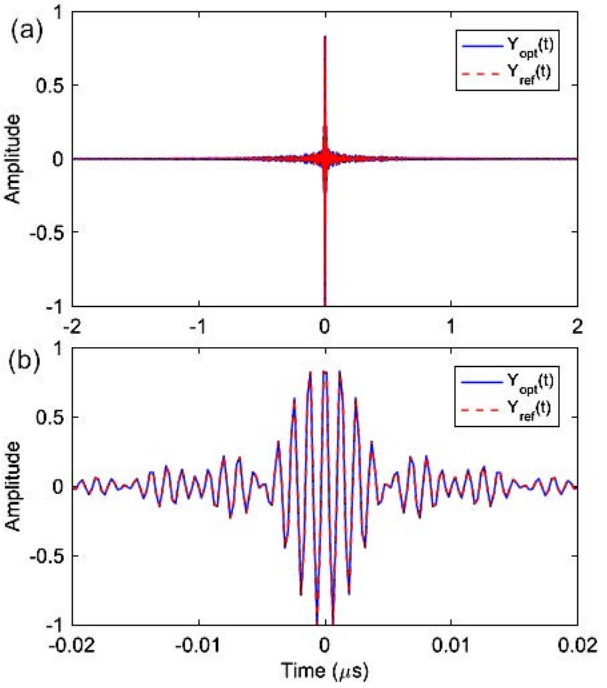

FIGURE 3. a) Synthetic comparison of the normalized intensity focusing of the GWS operator (blue solid line) with that of TR (red dashed line). b) Zoom of the comparison between -0.02 μs and 0.02 μs. The duration of the focusing pulse is about 10 *ns*.

B. IN-SITU MEASUREMENTS

Now that our approach has been validated with synthetic signals in computer simulations based on measured scattering matrices, we inject temporally on the antenna array the $N = 5$ time signals composing the vector $\psi_{\text{opt}}(t)$. These in-situ

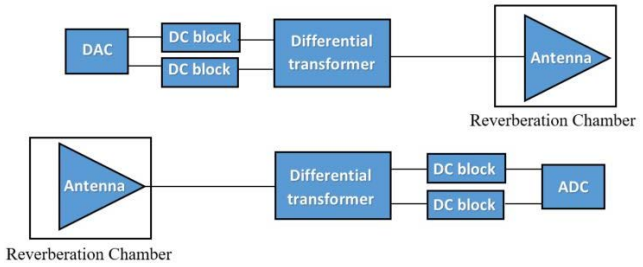

FIGURE 4. Drawing of the connection between the FPGA and the antennas showing the different components, especially the DC block and the differential transformer. They show the connection from ADC to an antenna (top) and from an antenna to DAC (bottom).

measurements are performed with a field programmable gate array (FPGA) of type Zynq UltraScale radiofrequency system on chip (RFSoc) ZCU111 of Xilinx. This type of FPGA has 8 Digital-to-Analog Converters (DACs) and 8 Analog-to-Digital Converters (ADCs), with data rates of 4.096 GS/s (12 bits) and 6.554 GS/s (14 bits), respectively. Each of these converters can work independently. However, it is also possible to synchronize them all (this is the case in our experiment). To do so, the capacities of the DACs and ADCs are limited to a sampling frequency of $F_s = 3.93$ GS/s and the number of samples must be a multiple of 32. Our incoming wavefronts are sampled over 15744 data points with a sampling time $T_s = 1/F_s$. A maximal time window of 4 μs must be respected while the time-domain incoming wavefronts are defined.

The ADCs and DACs are connected to the antennas through an AES-LPA-502-G daughter board manufactured by Avnet. This connection is made via a direct-current block to limit the current feedback to the board. A differential transformer is then used to match the board's differential mode outputs to the antenna standard mode inputs as shown on Fig. 4. The FPGA is controlled by an Ethernet connection through a Matlab graphical interface to transmit and measure the signals. Measurements are performed after calibration (time-delay correction) of the DACs against a reference DAC.

The five injection sources are connected from DAC #1 to DAC #5 of the FPGA to transmit the time domain signals; the receiver is connected to an ADC. As expected, the signals are compressed in time and space into a short pulse of high amplitude at the receiver. We measure a 21 dB increase of the maximal amplitude on the target relative to a random incoming time signal of the same amplitude (see Fig. 5(a)).

To further enhance the amplitude at the focus, we also perform one-bit time reversal based on $\psi_{\text{opt}}(t)$. One-bit TR consists in switching the input temporal signal between ± 1 according to the sign of $\psi_{\text{opt}}(t)$ [12], [13], [14]. The result shown in Fig. 5(b) gives a gain of 7.3 dB obtained with the one-bit technique. We have therefore demonstrated through in-situ measurements that the GWS operator provides excellent results also in the time domain so that MISO precoding schemes without the direct knowledge of the CSI can be implemented.

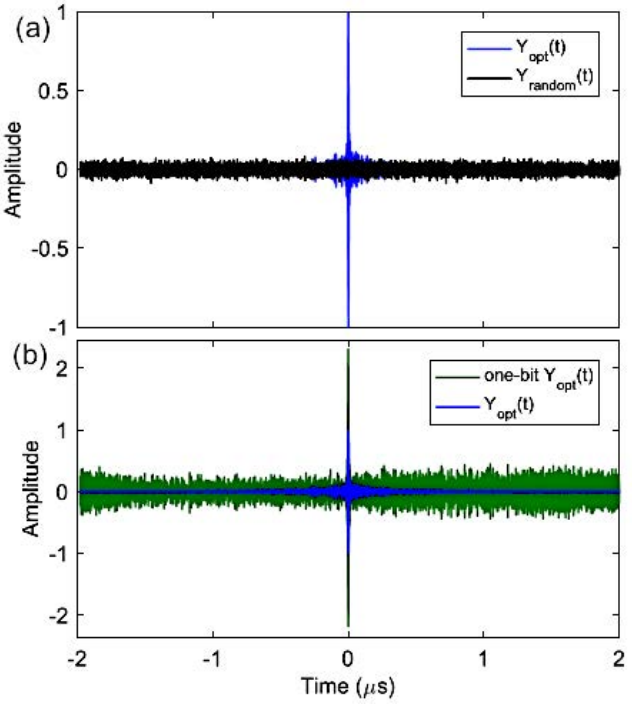

FIGURE 5. a) Focused signal compressed in time obtained by injecting $\psi_{\text{opt}}(t)$ (blue solid line). In comparison, injecting random incoming signals that are also normalized in the frequency domain (black solid line) provides a maximum amplitude 12 times smaller. b) Time-domain signals measured upon injecting $\psi_{\text{opt}}(t)$ (blue solid line) and the corresponding one-bit signal (green solid line).

In MISO-TR techniques [34], increasing the number of transmitting antennas provides higher amplitude pulses and thereby reduces the inter-symbol interference given that the transmitted fields are uncorrelated [35], [36].

In Fig. 6(a), we verify that the focused intensity found from the GWS operator also increases linearly with the number of transmitting antennas N [11]. To this end, we determine the optimal incoming wavefront $\psi_{\text{opt}}(\omega)$ from measurements of the $N \times N$ scattering matrix by selecting N antennas among the five available ones ($1 < N < 5$). The corresponding focused intensity $Y^2_{\text{opt}}(t)$ is in agreement with the theoreticaly prediction with a tolerance range between 1.15 % and 16.61 %.

Next, we explore the sensitivity of our CSI-estimation approach to the noise level during the CSI estimation. We define two signal-to-noise ratios (SNRs) as:

$$\text{SNR}_1 = \frac{\|S_1\|}{\sigma \|\mathcal{N}\|}, \tag{8}$$

and

$$\text{SNR}_2 = \frac{\|\Delta S\|}{\sigma \|\mathcal{N}\|}. \tag{9}$$

The SNRs are averaged over the frequency range. The first definition is the standard definition of SNR because it relates to physical measured signals (the scattering matrix). The second definition is based on parameters that cannot be

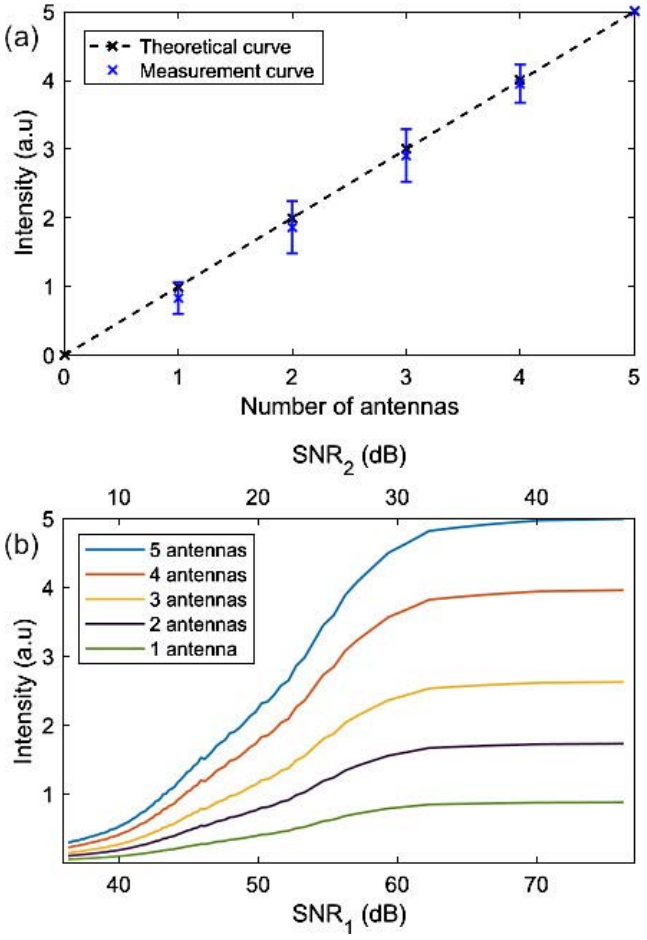

FIGURE 6. (a) Intensity as a function of the number of transmitting antennas. The blue data points show the results from our experiments. The black dashed line shows a linear fit. (b) Intensity as a function of SNR for different numbers of transmitting antennas. "SNR_1" is calculated based on S_1 while "SNR_2" is calculated based on ΔS (see discussion in text). The intensities are defined as the maximum of the envelope of the focused pulse and normalized by the average focused intensity obtained with one transmitting antenna.

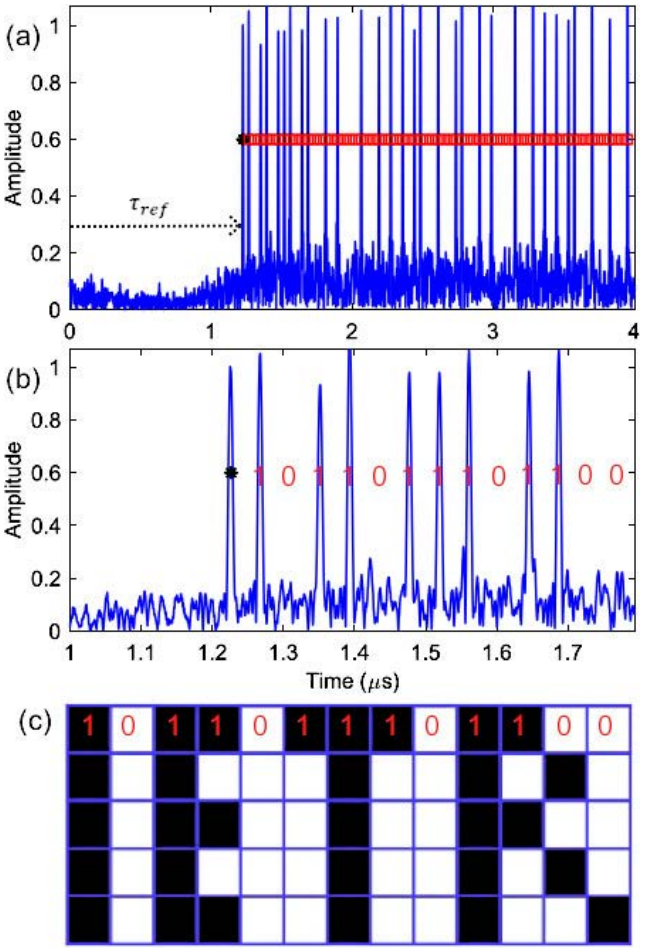

FIGURE 7. (a) Picture of the 65 *bits* plus the reference bit in black asterisk transmitted to the receiver. τ_{ref} denotes the necessary time to transmit the reference pulse for decoding. (b) Zoom on the first thirteen entries of the sequence of transmitted information. A bit value of 1 corresponds to the presence of a pulse, and a value of 0 to its absence at each τ. (c) Decoded received information: our laboratory's name (IETR) is correctly reconstructed.

directly measured but are obtained by processing independent measurements of the two physical signals (the modification of the scattering matrix due to the impedance change). The second definition yields hence a more universal result in that it removes the impact of the target's scattering cross-section.

For $N = 1, .., 5$ we simulate the impact of the noise level by adding to the scattering matrices $S_1(\omega)$ and $S_2(\omega)$ a Gaussian noise $\sigma\mathcal{N}$, at each frequency on the 10^4 points of the sampled bandwidth. Here, $\mathcal{N}$ denotes the standard normal distribution, its elements are normally distributed complex random numbers and σ is defined as $\sigma = 0 \rightarrow 10^{-3}$ over 100 points. For each value of σ, we average the focused intensity over 1000 realizations of the noise matrices. The focused intensity presented in Fig. 6(b) reaches its maximum value at $SNR_2 \sim 30$ dB and $SNR_1 \sim 60$ dB. It is clear that our CSI-estimation technique relies on measuring a minute change of the scattering matrix, such that the calibration measurements must be performed at a sufficiently good SNR. Figure 6(b) also shows that incorporating more antennas does not degrade the SNR but only increases the focusing intensity by a factor N. Results from a MISO-GWS operator therefore clearly outperform those of a SISO-GWS operator.

C. IMAGE TRANSMISSION

In this last section, we show that our approach enables wireless MISO communications. We aim to transmit a black and white picture with a size of 13 × 5 pixels representing the name of our laboratory (IETR). Black pixels are associated with bits $b = 1$ whereas white pixels correspond to bits $b = 0$. We use a Binary Amplitude Shift Keying (BASK) modulation to transmit the information. A first pulse representing the reference time delay is also added resulting in a total of 66 bits to transmit. We define the vector of pulse trains $\psi_{\text{im}}(t)$ as

$$\psi_{\text{im}}(t) = \sum_{n=1}^{66} b_n \psi_{\text{opt}}(t + n\tau), \tag{10}$$

where τ is the time delay between each pulse. The time delay associated with the arrival of the decoding pulse is equal

to $\tau_{\text{ref}} = 1.23\ \mu$s and the FPGA time window is set to 4 μs. In order to transmit the 66 bits within a single frame, we choose $\tau = 40$ ns. This ensures that i) τ is four times the pulse duration ($\delta t \sim 10\ n$s) to avoid any overlap between the received pulses and ii) the duration of $\psi_{\text{im}}(t)$ is smaller than the maximal FPGA time window. The received signal when injecting $\psi_{\text{im}}(t)$ and a zoom on the beginning of the signal are shown in Fig. 7(a,b). The decoding of the transmitted information starts with the presence of the first pulse. The 65 bits are then identified at each time interval τ with a simple level cut-off as decoding decision. Our information is accurately transmitted and the image is perfectly reconstructed (see Fig. 7(c)). In this way, we have accurately transmitted an information to the receiver without directly communicating with the receiver.

The bit-error-rate analysis of our scheme is directly equivalent to that of TR schemes already studied in the literature [37]. The only difference between our scheme and a TR scheme with respect to noise is the impact of noise on the channel estimation step, the channel estimation being the main contribution of our paper. This analysis was provided in the previous section (see Fig. 6(b)). Of course, for our image-transmission demonstration we estimated the channel benefiting from our vector network analyzer's great dynamic range, so our CSI estimate was close-to-perfect and hence the transmission was flawless.

IV. CONCLUSION

We have presented a new approach for wireless communications exploiting precoding schemes without the need of a direct measurement of the CSI. We have demonstrated that the transfer functions between an antenna array and a receiver can be accurately estimated from the modulation of the receiver's impedance using an approach based on the GWS operator. While the technique was first introduced for narrowband signals, we have extended it to the time domain by correcting the global phase. We have shown that the reconstructed time signals provide the same focusing performance as a TR experiment. The in-situ experiments carried out in a reverberation chamber illustrate that the technique is efficient in complex media and is not limited by multiple scattering. We further showed the possibility to transmit an information to the receiver with simple precoding and decoding schemes. Although our experiment is performed for MISO precoding schemes, it can be extended to MIMO techniques; this would require that the receiving antennas modulate their impedances in a synchronized manner, one at a time. Our indirect CSI-estimation technique may find applications in communications and power transfer, for applications ranging from the biomedical sector to electronic warfare. For the latter, it will be important to drastically increase the transmitted power.

REFERENCES

[1] T. K. Y. Lo, "Maximum ratio transmission," *IEEE Trans. Commun.*, vol. 47, no. 10, pp. 1458–1461, Oct. 1999.

[2] R. W. Lucky, "Automatic equalization for digital communication," *Bell Syst. Tech. J.*, vol. 44, no. 4, pp. 547–588, Apr. 1965.

[3] H. Bolcskei, "MIMO-OFDM wireless systems: Basics perspectives and challenges," *IEEE Wireless Commun.*, vol. 13, no. 4, pp. 31–37, Aug. 2006.

[4] M. Fink, "Time reversal of ultrasonic fields. I. Basic principles," *IEEE Trans. Ultrason., Ferroelectr., Freq. Control*, vol. 39, no. 5, pp. 555–566, Sep. 1992.

[5] G. Lerosey, J. de Rosny, A. Tourin, A. Derode, G. Montaldo, and M. Fink, "Time reversal of electromagnetic waves," *Phys. Rev. Lett.*, vol. 92, no. 19, May 2004, Art. no. 193904.

[6] T. Strohmer, M. Emami, J. Hansen, G. Papanicolaou, and A. J. Paulraj, "Application of time-reversal with MMSE equalizer to UWB communications," in *Proc. IEEE GLOBECOM*, vol. 5, Nov./Dec. 2004, pp. 3123–3127.

[7] P. Kyritsi, G. Papanicolaou, P. Eggers, and A. Oprea, "Time reversal techniques for wireless communications," in *Proc. IEEE 60th Veh. Technol. Conf.*, vol. 4, Jun. 2004, pp. 47–51.

[8] I. H. Naqvi, G. El Zein, G. Lerosey, J. de Rosny, P. Besnier, A. Tourin, and M. Fink, "Experimental validation of time reversal ultra wide-band communication system for high data rates," *IET Microw., Antennas Propag.*, vol. 4, no. 5, pp. 643–650, May 2010.

[9] G. Lerosey, J. de Rosny, A. Tourin, and M. Fink, "Focusing beyond the diffraction limit with far-field time reversal," *Science*, vol. 315, no. 5815, pp. 1120–1122, 2007.

[10] C. Oestges, A. D. Kim, G. Papanicolaou, and A. J. Paulraj, "Characterization of space-time focusing in time-reversed random fields," *IEEE Trans. Antennas Propag.*, vol. 53, no. 1, pp. 283–293, Jan. 2005.

[11] R. C. Qiu, C. Zhou, N. Guo, and J. Q. Zhang, "Time reversal with MISO for ultrawideband communications: Experimental results," *IEEE Antennas Wireless Propag. Lett.*, vol. 5, pp. 269–273, 2006.

[12] A. Derode, A. Tourin, and M. Fink, "Ultrasonic pulse compression with one-bit time reversal through multiple scattering," *J. Appl. Phys.*, vol. 85, no. 9, pp. 6343–6352, May 1999.

[13] P. Kyritsi and G. Papanicolaou, "One-bit time reversal for WLAN applications," in *Proc. IEEE 16th Int. Symp. Pers., Indoor Mobile Radio Commun.*, Sep. 2005, pp. 532–536.

[14] D. Abbasi-Moghadam and V. T. Vakili, "A SIMO one-bit time reversal for UWB communication systems," *EURASIP J. Wireless Commun. Netw.*, vol. 2012, no. 1, p. 113, Mar. 2012.

[15] J. Feng, C. Liao, L. L. Chen, and H. J. Zhou, "Amplification of electromagnetic waves by time reversal mirror in a leaky reverberation chamber," in *Proc. Microw. Millim. Wave Technol. (ICMMT)*, 2012, pp. 1–4.

[16] D. J. Love and R. W. Heath, Jr., "Equal gain transmission in multiple-input multiple-output wireless systems," *IEEE Trans. Commun.*, vol. 51, no. 7, pp. 1102–1110, Jul. 2003.

[17] T. Dubois, M. Crussiere, and M. Helard, "On the use of time reversal for digital communications with non-impulsive waveforms," in *Proc. 4th Int. Conf. Signal Process. Commun. Syst.*, Dec. 2010, pp. 1–6.

[18] T. Dubois, M. Hélard, M. Crussière, and C. Germond, "Performance of time reversal precoding technique for MISO-OFDM systems," *EURASIP J. Wireless Commun. Netw.*, vol. 2013, no. 1, pp. 1–16, Nov. 2013.

[19] M. Maaz, M. Hélard, P. Mary, and M. Liu, "Performance analysis of time-reversal based precoding schemes in MISO-OFDM systems," in *Proc. IEEE Veh. Technol. Conf. (VTC Spring)*, May 2015, pp. 1–6.

[20] A. Shaikh and M. J. Kaur, "Comprehensive survey of massive MIMO for 5G communications," in *Proc. Adv. Sci. Eng. Technol. Int. Conf. (ASET)*, Mar. 2019, pp. 1–5.

[21] F. T. Smith, "Lifetime matrix in collision theory," *Phys. Rev.*, vol. 118, no. 1, pp. 349–356, Apr. 1960.

[22] E. P. Wigner, "Lower limit for the energy derivative of the scattering phase shift," *Phys. Rev.*, vol. 98, no. 1, pp. 145–147, Apr. 1955.

[23] P. Ambichl, A. Brandstötter, J. Böhm, M. Kühmayer, U. Kuhl, and S. Rotter, "Focusing inside disordered media with the generalized Wigner-Smith operator," *Phys. Rev. Lett.*, vol. 119, no. 3, Jul. 2017, Art. no. 033903.

[24] M. Horodynski, M. Kühmayer, A. Brandstötter, K. Pichler, Y. V. Fyodorov, U. Kuhl, and S. Rotter, "Optimal wave fields for micromanipulation in complex scattering environments," *Nature Photon.*, vol. 14, no. 3, pp. 149–153, Mar. 2020.

[25] S. Rotter, P. Ambichl, and F. Libisch, "Generating particlelike scattering states in wave transport," *Phys. Rev. Lett.*, vol. 106, no. 12, Mar. 2011, Art. no. 120602.

[26] J. Carpenter, B. J. Eggleton, and J. Schröder, "Observation of Eisenbud–Wigner–Smith states as principal modes in multimode fibre," *Nature Photon.*, vol. 9, no. 11, pp. 751–757, 2015.
[27] M. Durand, S. M. Popoff, R. Carminati, and A. Goetschy, "Optimizing light storage in scattering media with the dwell-time operator," *Phys. Rev. Lett.*, vol. 123, no. 24, Dec. 2019, Art. no. 243901. [Online]. Available: https://journals.aps.org/prl/abstract/10.1103/PhysRevLett.123.243901
[28] P. del Hougne, R. Sobry, O. Legrand, F. Mortessagne, U. Kuhl, and M. Davy, "Experimental realization of optimal energy storage in resonators embedded in scattering media," *Laser Photon. Rev.*, vol. 15, no. 3, Mar. 2021, Art. no. 2000335.
[29] U. R. Patel and E. Michielssen, "Wigner–Smith time-delay matrix for electromagnetics: Theory and phenomenology," *IEEE Trans. Antennas Propag.*, vol. 69, no. 2, pp. 902–917, Feb. 2020.
[30] U. R. Patel and E. Michielssen, "Wigner–Smith time delay matrix for electromagnetics: Computational aspects for radiation and scattering analysis," *IEEE Trans. Antennas Propag.*, vol. 69, no. 7, pp. 3995–4010, Jul. 2021.
[31] P. del Hougne, K. B. Yeo, P. Besnier, and M. Davy, "Coherent wave control in complex media with arbitrary wavefronts," *Phys. Rev. Lett.*, vol. 126, no. 19, May 2021, Art. no. 193903.
[32] K. B. Yeo, M. Davy, and P. Besnier, "Non-invasive optimal coupling upon detection of a local change of impedance in a cable network," in *Proc. IEEE Int. Joint EMC/SI/PI EMC Eur. Symp.*, May 2021, vol. 10, no. 3, pp. 528–532.
[33] D. A. Hill, "Plane wave integral representation for fields in reverberation chambers," *IEEE Trans. Electromagn. Compat.*, vol. 40, no. 3, pp. 209–217, Aug. 1998.
[34] X. Zhou, P. C. F. Eggers, P. Kyritsi, J. B. Andersen, G. F. Pedersen, and J. O. Nilsen, "Spatial focusing and interference reduction using MISO time reversal in an indoor application," in *Proc. IEEE/SP 14th Workshop Stat. Signal Process.*, Aug. 2007, pp. 307–311.
[35] A. Cozza and F. Monsef, "Multiple-source time-reversal transmissions in random media," *IEEE Trans. Antennas Propag.*, vol. 62, no. 8, pp. 4269–4281, Aug. 2013.
[36] G. Lerosey, J. de Rosny, A. Tourin, A. Derode, and M. Fink, "Time reversal of wideband microwaves," *Appl. Phys. Lett.*, vol. 88, no. 15, 2006, Art. no. 154101.
[37] H. T. Nguyen, J. B. Andersen, G. F. Pedersen, P. Kyritsi, and P. C. F. Eggers, "Time reversal: A measurement-based investigation," *IEEE Trans. Wireless Commun.*, vol. 5, no. 8, pp. 2242–2252, Aug. 2006, doi: 10.1109/TWC.2006.1687740.

K. BRAHIMA YEO was born in Bouake, Ivory Coast. He received the M.S. degree in electromagnetic compatibility (EMC) from the University of Clermont Auvergne, France, in 2019. He is currently pursuing the Ph.D. degree in electronics with the Institut d'Electronique et des Technologies du numéRique, INSA of Rennes, Rennes, France. He worked on the wavefront control for remote reverberation chamber and multipath communication scenarios.

CECILE LECONTE received the degree in electrical engineering from the National Institute of Applied Sciences of Rennes, in 2001. Prior to her academic career, she had been working for several years in CADIMES, involved in RFID systems test and measurement. She is currently working with the Institut d'Electronique et des Technologies du Numérique (IETR) on electronic systems development applied to remote sensing.

PHILIPP DEL HOUGNE (Member, IEEE) is a tenured CNRS researcher affiliated with the Université de Rennes 1, France. He graduated in physics from Imperial College London, U.K., and was awarded a doctorate by Université Sorbonne Paris Cité, France. He subsequently held postdoctoral positions in Nice and Rennes, France, and Lausanne, Switzerland.

He currently leads the research on Intelligent Wave Systems at CNRS – IETR (Université de Rennes 1), France, which combines programmable-metamaterial hardware with artificial-intelligence algorithms and mesoscopic-scattering theory to mold the flow of information through tailored wave-matter interactions for information extraction (imaging, sensing, localization), information processing (analog wave-based computing), and information transfer (wireless communications).

PHILIPPE BESNIER (Senior Member, IEEE) received the Diplôme d'Ingénieur degree in electronics from the École Universitaire d'Ingénieurs de Lille (EUDIL), Lille, France, in 1990, and the Ph.D. degree in electronics from the University of Lille, in 1993. Following a one-year period at the ONERA, Meudon, as an Assistant Scientist with the EMC Division, he was with the Laboratory of Radio-Propagation and Electronics (LRPE), University of Lille, as a Researcher (Chargé de Recherche) at the Centre National de la Recherche Scientifique (CNRS), from 1994 to 1997. From 1997 to 2002, he was the Director of the Centre d'Etudes et de Recherches en Protection Electromagnétique (CERPEM): a not-for-profit organization for research, expertise and training in EMC and related activities, based in Laval, France. He also co-founded and headed TEKCEM, in 1998, a small business company specialized in turn-key systems for EMC measurements. Back to CNRS, in 2002, he has been since then with the Institut d'Electronique et des Technologies du numéRique (IETR), Rennes, France (www.ietr.fr). He was the Co-Head of the "Antennas and Microwave Devices" Research Department, IETR, from 2012 to 2016. He was appointed as a CNRS Senior Researcher (Directeur de Recherche au CNRS), in 2013. He headed the WAVES (now eWAVES) Team–electromagnetic waves in complex media, during the first semester of 2017. Since July 2017, he has been the Deputy Director of the IETR. His research activities deal with interference analysis on cable harnesses (including electromagnetic topology), theory and application of reverberation chambers, shielding and absorbing techniques, quantification and propagation of uncertainties in EMC modeling and electromagnetic cybersecurity.

MATTHIEU DAVY received the Diplôme d'Ingénieur degree from the École Centrale de Lille, Lille, France, in 2007, and the Ph.D. degree from the University of Paris Diderot, in 2010. He subsequently held postdoctoral positions with the Queen's college, City University of New York, USA; and the Institut Langevin, Paris, France. He was the Co-Head of the SHINE Team, from 2019 to 2022, and now heads the "Wave and Signals" Research Department, IETR, since 2022. He has been a Junior Member of the Institut Universitaire de France, since 2019. He is currently an Assistant Professor at the University of Rennes 1 and is affiliated to the Institut d'Electronique et des Technologies du numéRique (IETR), Rennes, France (www.ietr.fr). His research activities are dedicated to the understanding and control of wave propagation in disordered environments, including random and chaotic systems, for applications in wireless communications, computational imaging, and electromagnetic compatibility.